Journal of Inorganic and Organometallic Polymers and Materials
https://doi.org/10.1007/s10904-024-03089-1

RESEARCH

Zn(II)-Coordination Polymers Constructed from Isomeric Bis(Imidazole) Derivative Ligands and Tetracarboxylic Acid for the Detection of Iron Ions

Enes Kavak[1] · Melike Şevik[1] · Ayça Aydoğan[1] · Sevde Demir[1] · Gökhan Solmaz[2] · Fatih Semerci[3] · Hakan Erer[1] · Okan Zafer Yeşilel[1] · Mürsel Arıcı[1]

Received: 15 January 2024 / Accepted: 27 March 2024

Abstract
Three Zn(II)-coordination polymers, namely, $\{[Zn_2(\mu_4\text{-L})(\mu\text{-obix})_2]\cdot 4DMF\}_n$ (**1**), $\{[Zn_2(\mu_4\text{-L})(\mu\text{-mbix})_2]\cdot 6H_2O\}_n$ (**2**) and $\{[Zn_2(\mu_4\text{-L})(\mu\text{-pbix})_2]\cdot 5H_2O\}_n$ (**3**), (L^{4-}: 5,5'-(terephthaloylbis(azanediyl))diisophthalate and obix (y = 2), mbix (y = 3), pbix (y = 4): 1,y-bis((1*H*-imidazol-1-yl)methyl)benzene) were prepared with a tetracarboxylic acid and flexible isomeric bis(imidazole) linkers and characterized. The compounds displayed structural diversity depending on the rotation of imidazole rings around the $-CH_2-$ groups on bis(imidazole) ligands. Compounds **1–3** showed 2-fold interpenetrated 3D framework, 2D structure and 3D framework, respectively. The compounds showed high emissions in solid-state and solutions. Luminescence experiments showed that compounds **1–3** displayed sensitive detection towards Fe^{3+} ions with detection limits of 2.31 ppm, 5.17 ppm and 2.61 ppm, respectively. Moreover, the compounds could selectively detect Fe^{3+} ions over the other interfering metal ions via luminescence quenching. The detection mechanism could be ascribed to the competitive light absorption between Fe^{3+} ions and the compounds.

Keywords Fe^{3+} Detection · Structural Diversity · Isomeric bis(Imidazole) Ligands

1 Introduction

Periodic assembly of metal ions and multitopic bridging ligands results in the formation of coordination polymers with well-defined crystalline structures [1–3]. Coordination polymers attract attention due to their diverse applications in adsorption and separation processes, heterogeneous catalysis, and electrochemical energy storage [4–9]. Applications for coordination polymers are strongly influenced by the compositions of metal ions, anionic and neutral organic ligands with different functional sites and flexibilities, as well as by the characteristics of topological structures of the final material [10].

Fe^{3+} is essential for the human body, supporting metabolism and participating in key physiological functions such as coordinating brain activity, transferring oxygen, and producing hemoglobin [11–13]. However, an imbalance can lead to significant health issues. For example, insufficient iron may compromise immunity, while excess iron can contribute to diseases like cancer, liver problems, and heart conditions [14]. The expansion of industries like electronics, electroplating, and chemicals has elevated metal ion levels in freshwater, posing potential risks to human health. With this motivation, the researchers are actively working on developing precise and rapid detection methods for Fe^{3+} ions [15].

Luminescent coordination polymers are currently of great interest, particularly because of their high sensitivity to heavy metal ion detection [16, 17]. In contrast to conventional fluorescent sensors, luminescent coordination polymers exhibit advantages in detecting Fe^{3+} and various hazardous

✉ Mürsel Arıcı
marici@ogu.edu.tr

1 Department of Chemistry, Faculty of Science, Eskişehir Osmangazi University, Eskişehir 26480, Türkiye

2 Central Research Laboratory Application and Research Center (ARUM), Eskişehir Osmangazi University, Eskişehir 26480, Türkiye

3 Department of Energy Systems Engineering, Faculty of Technology, Kırklareli University, Kırklareli 39000, Türkiye

Published online: 30 April 2024

compounds due to their design flexibility, high porosity, and adjustable structure achieved through the careful selection of building blocks [18, 19]. Several coordination polymers were reported as promising luminescence-based sensors for the detection of Fe^{3+} ions [20–24]. As seen in the previous studies, Fe^{3+} ions can selectively and sensitively change the luminescence emission of coordination polymers, providing advantages in response time, and robust anti-interference performance [25]. Moreover, it is possible to build the coordination polymer's assembly for luminescence-based sensor applications by consciously selecting transition metal ions and organic bridging ligands. Despite an abundance of studies on coordination polymers' Fe^{3+} sensing capabilities, a more thorough study is still necessary to comprehend the underlying mechanisms and explore potential applications. In these coordination polymers, Zn(II) ions, characterized by a d^{10} electronic configuration, exhibit a lack of reactivity in redox reactions [26]. They represent promising sources of transition metal ions, pairing them with flexible emitting organic ligands, to construct luminescent coordination polymers. These materials serve as effective fluorescence-based chemical sensors for the detection of Fe^{3+}. Nevertheless, the limited stability of coordination polymers in aqueous environments often restricts their effectiveness in sensing target metal ions. To date, only a limited number of coordination polymer-based sensors have been reported to maintain stability in water [27, 28]. Consequently, enhancing the water stability of the sensors has consistently posed a significant challenge.

In this context, we have recently made contributions to the scientific community by synthesizing several water-stable luminescence coordination polymers using Zn(II) and Cd(II) ions in combination with dual-bridging organic ligands [8, 13, 29]. These materials show promise as multifunctional sensing agents, offering sensitive and selective detection capabilities for Fe^{3+} and hazardous compounds. Motivated by the mentioned points, new luminescent coordination polymers in single crystal forms, denoted as $\{[Zn_2(\mu_4\text{-L})(\mu\text{-obix})_2]\cdot 4DMF\}_n$ (**1**), $\{[Zn_2(\mu_4\text{-L})(\mu\text{-mbix})_2]\cdot 6H_2O\}_n$ (**2**) and $\{[Zn_2(\mu_4\text{-L})(\mu\text{-pbix})_2]\cdot 5H_2O\}_n$ (**3**), were synthesized via solvothermal methods, employing the isomeric bis(imidazole) derivative ligands and Zn(II) ions in the presence of 5,5'-(terephthaloylbis(azanediyl))diisophthalic acid (H_4L) (Scheme 1). The Fe^{3+} sensing properties of the well-characterized luminescent material were further investigated. The sensing properties of the compounds for the detection of Fe^{3+} ions in solutions were discussed in detail.

2 Materials and Measurements

The chemicals were procured commercially except that H_4L and bis(imidazole) derivative linkers were obtained according to the literature [30, 31]. The physical measurements and the experimental procedures of luminescence studies were given in the supplementary information file.

2.1 Syntheses

2.1.1 $\{[Zn_2(\mu_4\text{-L})(\mu\text{-obix})_2]\cdot 4DMF\}_n$(1)

H_4L (0.049 g, 0.1 mmol), obix (0.024 g, 0.01 mmol) and $Zn(NO_3)_2\cdot 6H_2O$ (0.06 g, 0.02 mmol) were stirred in the mixture of DMF: H_2O (9:3, 12 mL) for 30 min and 2 drops of 6.0 M HNO_3 were introduced into the previous mixture, resulting in a clear solution. The resulting mixture was placed in a sealed bottle (20 mL) and subjected to heating at 85ºC for 3 days to obtain colorless crystals. Yield: 56% based on H_4L. Anal. Calcd. for $C_{32}H_{34}N_7O_7Zn$: C, 55.38; H, 4.94; N, 14.13%. Found: C, 55.74; H, 4.51; N, 14.06%. FT-IR (KBr, cm^{-1}): 3265 m, 3138 m, 3119 m, 2936 w, 1668 s, 1624 s, 1566 vs., 1406 s, 1358 s, 1236 m, 1097 m, 727 s.

2.1.2 $\{[Zn_2(\mu_4\text{-L})(\mu\text{-mbix})_2]\cdot 6H_2O\}_n$(2)

The synthesis of **2** was as outlined for **1**, except that mbix (0.024 g, 0.01 mmol) and $ZnCl_2$ (0.027 g, 0.02 mmol) were used instead of obix and $Zn(NO_3)_2\cdot 6H_2O$. Yield: 69% based

Scheme 1 The molecular structure of obix (**a**), mbix (**b**), pbix (**c**) and H_4L (**d**) used in the syntheses of the compounds

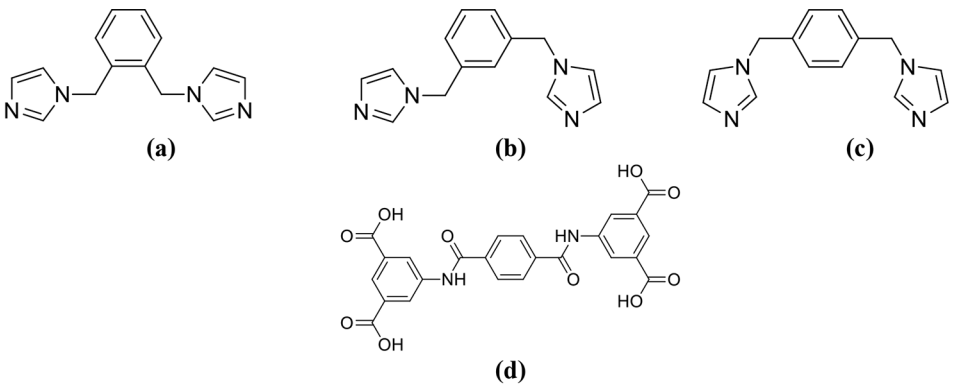

on H_4L. Anal. Calcd. for $C_{26}H_{26}N_5O_8Zn$: C, 51.88; H, 4.35; N, 11.64%. Found: C, 51.97; H, 4.21; N, 11.13%. FT-IR (KBr, cm^{-1}): 3424 s, 3292 m, 3140 m, 3047 w, 2988 m, 1663 s, 1620 s, 1572 vs., 1433 s, 1356 s, 1282 s, 1086 m, 1045 w.

2.1.3 {[Zn_2(μ_4-L)(μ-pbix)$_2$]·5H_2O}$_n$(3)

A mixture of H_4L (0.049 g, 0.1 mmol), $Zn(NO_3)_2·6H_2O$ (0.06 g, 0.02 mmol) and pbix (0.024 g, 0.01 mmol) was stirred in a solution of DMA: H_2O (10:3, 13 mL) in the presence of 2 drops of 6.0 M HNO_3 for 30 min and then transferred into the sealed bottle (20 mL) and heated at 85°C for 2 days to obtain colorless crystals of **3**. Yield: 62% based on H_4L. Anal. Calcd. for $C_{52}H_{50}N_{10}O_{15}Zn_2$: C, 52.67; H, 4.25; N, 11.81%. Found: C, 52.48; H, 4.19; N, 11.23%. FT-IR (KBr, cm^{-1}): 3417 m, 3294 m, 3134 m, 3070 w, 1660 m, 1619 m, 1569 vs., 1528 s, 1428 s, 1338 vs., 1098 s, 949 m, 776 m.

3 Results and Discussion

3.1 Synthesis and Characterizations

Compounds **1–3** were solvothermally synthesized by the reaction of H_4L and isomeric bis(imidazole) derivative ligands in the presence of Zn(II) ions. They were characterized by several techniques. The amounts of C, H, N % of the compounds show the consistency with the assigned formula. In the FT-IR spectra of the compounds, ν(N-H) stretching vibration of L^{4-} ligand was observed in the range of 3265–3292 cm^{-1}. The peaks appearing in the range of 3140–2936 cm^{-1} were attributed to the aromatic and aliphatic ν(C-H) stretching vibrations. The symmetric and asymmetric stretchings related to the carboxylate groups of L^{4-} linker shifted to higher and lower wavelengths after connection to Zn(II) ions and appeared in the range of 1358–1338 cm^{-1} and 1566–1572 cm^{-1}, respectively.

Table 1 provides the crystal data and structure refinement parameters for the compounds. Additionally, selected bond lengths and angles were found in Tables S1, S2, S3. Crystallographic data for the structural analysis have been deposited with the Cambridge Crystallographic Data Centre, CCDC No. 1443933 and 1443934 for **1** and **2** and 2284664 for **3**.

3.1.1 {[Zn_2(μ_4-L)(μ-obix)$_2$]·4DMF}$_n$ (1)

X-ray structural analysis reveals that compound **1** adopts a monoclinic crystal structure within the space group $P2_1/n$. The molecular structure was shown in Fig. 1a. There are one zinc (II) centre, half 5,5'-(terephthaloylbis(azanediyl)) diisophthalate (L^{4-}), one obix ligand and two lattice DMF molecules in the asymmetric unit of compound **1**. As shown in Fig. 1a, Zn1 centre demonstrates distorted tetrahedral geometry ($\tau_4 = 0.907$), coordinated by two N atoms from two distinct obix ligands and two O atoms from carboxylates of two distinct L^{4-} ligands. The bond lengths between Zn and O/N atoms range from 1.9643(14) to 2.0444(17) Å. The coordination mode of L^{4-} ligand is *tetrakis*(*monodentate*) with the interisophthalate dihedral angle of 0.0° (through

Table 1 Crystal data and structure refinement parameters for compounds **1–3**

	1	2	3
Empirical formula	$C_{32}H_{34}N_7O_7Zn$	$C_{26}H_{26}N_5O_8Zn$	$C_{52}H_{48}N_{10}O_{15}Zn_2$
Formula weight	694.03	601.89	1183.74
Crystal system	Monoclinic	Monoclinic	Monoclinic
Space group	$P2_1/n$	$P2_1/n$	$P2_1/n$
a (Å)	9.4314 (5)	8.8781 (6)	9.1954 (5)
b (Å)	21.2241 (12)	16.1713 (9)	16.7195 (8)
c (Å)	16.7407 (8)	18.5083 (12)	18.2224 (10)
α (°)	90.00	90.00	90.00
β (°)	98.933 (2)	103.264 (3)	101.344 (2)
γ (°)	90.00	90.00	90.00
V (Å^3)	3310.4 (3)	2586.4 (3)	2746.8 (3)
Z	4	4	2
D_c (g cm^{-3})	1.393	1.546	1.431
μ (mm^{-1})	0.80	1.01	0.95
θ range (°)	3.1–27.7	3.1–27.8	2.3–23.5
Measured refls.	119,066	89,679	65,612
Independent refls.	8234	6450	5896
R_{int}	0.051	0.055	0.100
S	1.06	1.05	1.03
R1/wR2	0.039/0.099	0.037/0.093	0.079/0.256
$\Delta\rho_{max}/\Delta\rho_{min}$(eÅ^{-3})	0.60/-0.33	0.37/-0.43	1.35/-0.54

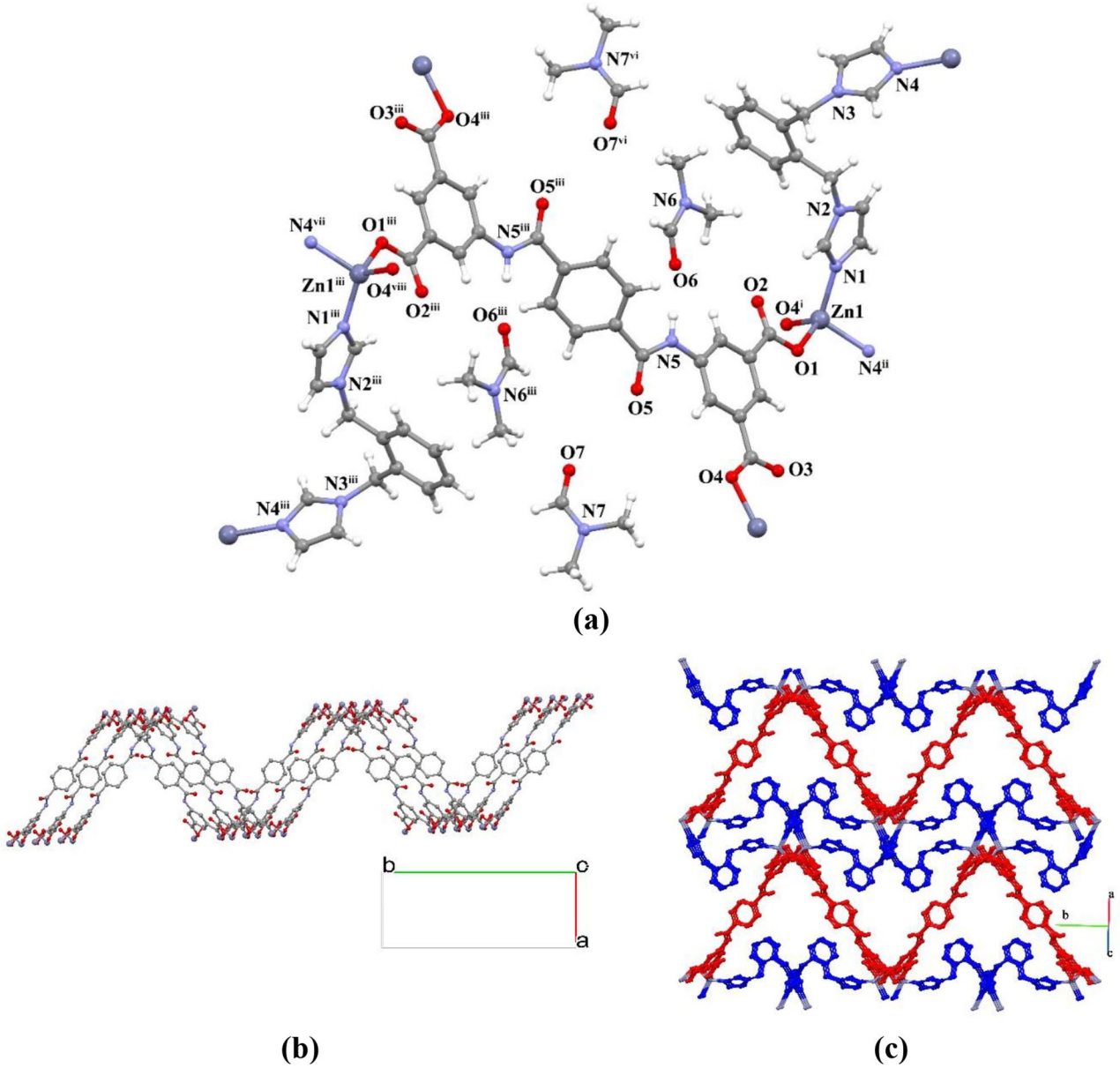

Fig. 1 (**a**) View of the molecular structure for **1** (**b**) View of the undulated 2D structure generated by L^{4-} and Zn(II) along ab layer in **1** (**c**) A view of 3D structure occurring by the connection of obix to 2D structure (obix and L^{4-} ligands were shown in blue and red colors, respectively in 3D structure)

C2–C3–C4–C5–C6–C7; $C2^{iii}$–$C3^{iii}$–$C4^{iii}$–$C5^{iii}$–$C6^{iii}$–$C7^{iii}$) (Fig. S1). The L^{4-} ligands bind to four zinc (II) centers, creating undulated 2D networks (Fig. 1b and Fig. S2) that include parallelogram voids with dimensions of 17.893•••20.132 Å (Zn•••Zn distances) and angles of 78.94° and 101.06° (Zn•••Zn•••Zn angle). In addition, two distinct obix linkers connect the neighboring undulated 2D networks, generating a 3D framework (Fig. 1c). 3D frameworks interpenetrate each other to form a 2-fold interpenetrating 3D framework with bbf topology (Fig. S3).

3.1.2 $\{[Zn_2(\mu_4\text{-L})(\mu\text{-mbix})_2]\cdot 6H_2O\}_n$ (2)

When mbix ligand was used instead of obix ligand, a 2D coordination polymer was obtained. It crystallizes in the monoclinic space group $P2_1/n$, and the asymmetric unit comprises half L^{4-} and one mbix ligands, one zinc (II) centre and three crystal water molecules (Fig. 2a). Zn(II) centres in compound **2** exhibit four coordination environment with the distorted tetrahedral ($\tau_4 = 0.87$) [32]. Zn(II) ions coordinate with two nitrogen atoms of two distinct mbix ligands and two carboxylate oxygen atoms of two

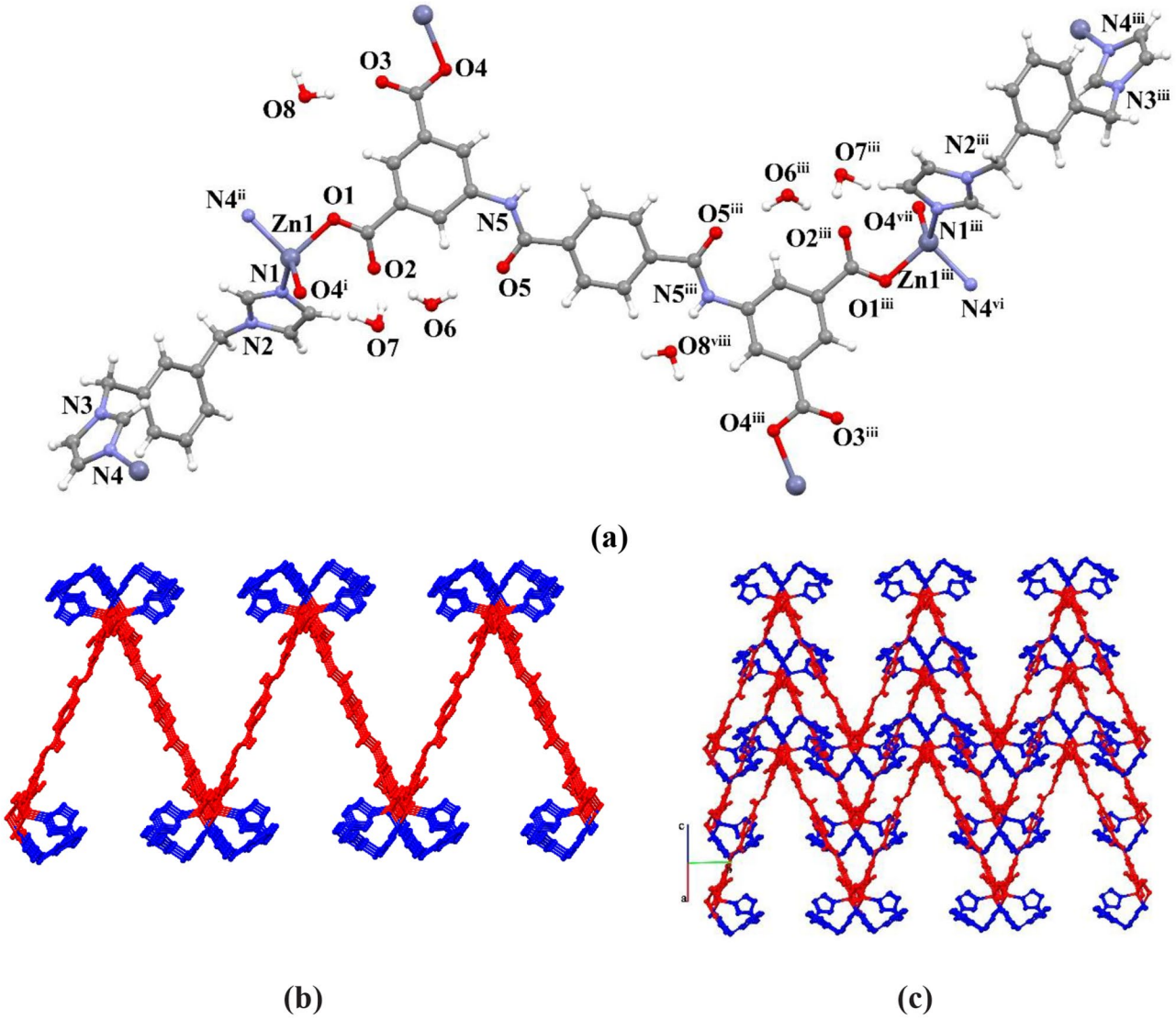

Fig. 2 **(a)** View of the molecular structure for **2** (**b**) 2D structure of **2** formed by L^{4-} ligands and Zn(II) ins (**c**) 2D stacking of **2** (mbix and L^{4-} ligands were shown in blue and red colors in the structures)

distinct L^{4-} ligands. The bond lengths of Zn-O/N span from 1.9767(15) to 2.0283(18) Å. The L^{4-} linker displays same coordination mode with compound **1**. The undulated 2D networks are generated through the coordination of zinc (II) centers and L^{4-} ligands, which contain parallelogram voids with dimensions of 18.600•••21.705 Å (Zn•••Zn distances) and angles of 56.20° and 123.80° (Zn•••Zn•••Zn angle) (Fig. S4a and Fig. S4b). The mbix ligands serves as bridging ligands between two Zn (II) centers and do not contribute to the dimensional aspects of the structure (Fig. 2b). However, it contributes to the stability of the two-dimensional structure. The mbix linker has an interimidazole dihedral angle of 86.77º. The distance between the Zn(II) centres bridged by the mbix linker is 9.406 Å. 2D structures are stacked to generate a 3D supramolecular structure (Fig. 2c). Compound **2** has a kagome (kgm) topology with a point symbol of $3^2.6^2.7^2$ (Fig. S4c).

3.1.3 $\{[Zn_2(\mu_4\text{-}L)(\mu\text{-}pbix)_2]\cdot 5H_2O\}_n$ (3)

In compound **3**, a 3D coordination polymer was obtained by using pbix linker, which has a high ability to form a 3D structure, as a bridging ligand. It crystallizes in the monoclinic crystal system with the space group of $P2_1/n$, and there are two different halves of pbix ligands, one Zn(II) centre, half L^{4-}, and two and a half lattice water molecules in the asymmetric unit (Fig. 3a). As demonstrated in Fig. 3a, Zn(II) centre displays distorted tetrahedral geometry ($\tau_4 = 0.91$), coordinated by two O atoms from the carboxylates of two distinct L^{4-} linkers and two N atoms from

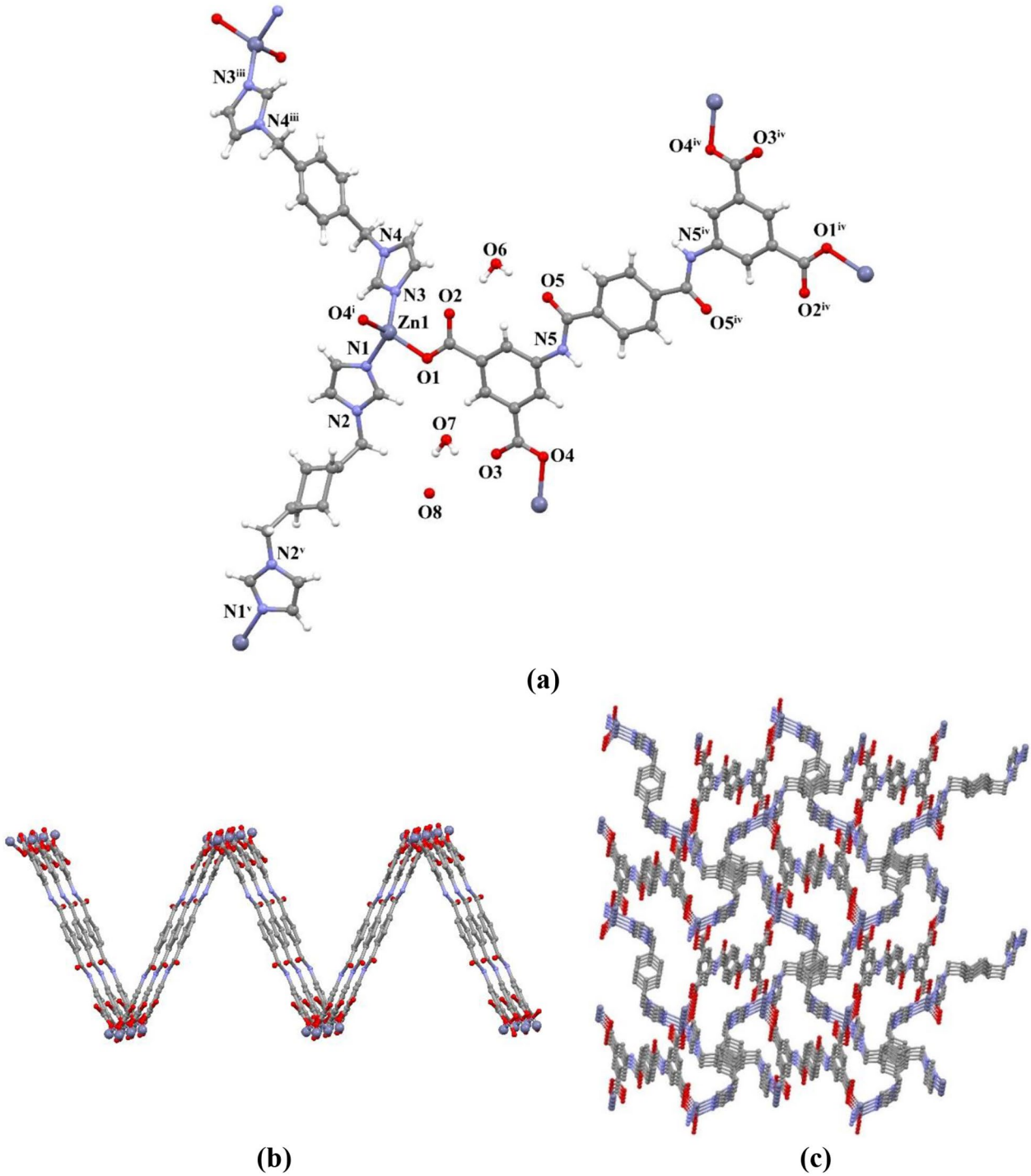

Fig. 3 (**a**) View of the molecular structure for **3** (**b**) 2D undulated network of **3** generated by L^{4-} and Zn(II) (**c**) 3D framework of **3**

two distinct pbix linkers. The bond lengths of Zn-O/N are in the range of 1.987(4)-2.012(5) Å. These bond lengths are compatible with the bond lengths of similar complexes found in the literature [13]. The coordination mode of L^{4-} ligand in compound **3** is similar to that observed in compounds **1** and **2**. The L^{4-} linkers connect to four zinc (II) ions, forming undulated 2D networks (Fig. 3b). Moreover, 3D framework is formed through the connection of two different pbix linkers to neighboring undulating 2D networks. (Fig. 3c). The distances between the Zn(II) centres bridged by the pbix linkers are 14.521 Å and 13.746 Å. Topological

analysis indicates that compound **3** displays a 4,2-connected 4,4T250 topology with the point symbol of 8^6 (Fig. S5).

PXRD patterns of the compounds were obtained to verify the phase purity. Experimental PXRD patterns of the compounds were identical to the simulated patterns obtained from SCXRD with the aid of the Mercury program, indicating that the bulk compounds possess phase purities (Fig. S6). Simultaneous thermal analysis curves were obtained in the temperature range of 30-800°C (Fig. S7, Fig. S8 and Fig. S9). For compound **1**, the initial weight loss of 19.0% was attributed to the elimination of DMF molecules (calc.: 21.0%). After this step, the compound displayed stability up to 380°C. Three water molecules with a weight of 9.0% in **2** and two and a half water molecules with a weight of 8.1% in compound **3** were removed in the temperature range of 30-125°C and 30-105°C, respectively (calc.: 8.97% for 2 and 7.60% for **3**). When further heating, the compounds were exothermally decomposed. The final possible products were ZnO (exp.: 10.86%, calc.: 11.67% for compound **1**; exp.: 15.3%, calc.: 13.47% for compound **2**; exp.: 11.0%, calc.: 13.67% for compound **3**).

N_2 adsorption desorption isotherms were recorded at 77 K to determine the BET surface areas of the compounds (Fig. S10). As seen in Fig. S10, the compounds display non-porous isotherm curves. The calculated BET surface areas of compounds **1–3**, 1.74 m^2/g, 1.86 m^2/g and 14.6 m^2/g, respectively. According to crystal result of **1**, although the compound seems to be porous, the instability of the framework is observed after removal of solvent molecules.

3.2 Structural Diversity

The compounds were synthesized under the same conditions with isomeric bis(imidazole) linkers. The compounds displayed structural diversity depending on bis(imidazole) linker. Compounds **1** and **3** showed 3D structures while compound **2** possessed a 2D structure. The structural differences between the dimensionality of the compounds were due to the flexibility of the bis(imidazole) linkers. Imidazole rings on the backbone of bis(imidazole) ligands can display *cis*- and *trans*-conformations with the rotation around the $–CH_2-$ groups. In the compounds, imidazole groups of bis(imidazole) ligands take place *trans*- position. The structural differences were due to the dihedral angles between imidazole and phenyl rings of bis(imidazole) ligands. The dihedral angles between imidazole rings in the obix, mbix and pbix ligands of the compounds were 85.24°, 86.77° and 0°, respectively. Due to the 0° of the dihedral angle between imidazole rings in the pbix, compound **3** has a 3D structure. In compounds **1** and **2**, the dihedral angles between imidazole and phenyl rings in the obix and mbix are 89.06° and 82°, 88.32° and 67.90°, respectively (Fig. S11). The low dihedral angles between imidazole and phenyl rings of mbix cause low dimensionality in compound **2** when compared to the other compounds.

3.3 Luminescence Studies

The luminescence coordination compounds have been drawn attention due to their usage as sensor materials. The solid-state luminescence spectra of the compounds and H_4L ligand were recorded under the same conditions. H_4L ligand exhibited emission at 446 nm upon excitation at 325 nm (Fig. S12). The emission could be assigned to $\pi^* \rightarrow \pi$ and $\pi^* \rightarrow n$ transitions. The emissions at 442 nm, 432 nm and 451 nm appeared for compounds **1–3**, respectively, upon excitation at 325 nm (Fig. S9). These emissions could be attributed to the intra-ligand transition of H_4L. The emission intensities of the compounds significantly increased when compared to the free ligand. This situation could be due to a decrease in the flexibility of the ligand after connection to metal centers [13]. The differences between emission intensities and wavelengths of the compounds could be due to the influence of bis(imidazole) linkers and the dimensionality of the final compounds. The emission behaviors of the compounds (2.0 mg) were evaluated in diverse solvents (3.0 mL) (Fig. S13) under the same conditions. The compounds showed diverse emission intensities depending on solvent molecules. Compound **1** displayed moderate emission in water. Moreover, compounds **2** and **3** displayed high emission intensities in water and methanol, respectively. Hence, the potential detection capabilities of the compounds towards metal ions were explored in water (for compounds **1** and **2**) and methanol (for compound **3**) solvents. PXRD patterns of the compounds after exposed to these solvents were recorded to check the stability of the compounds (Fig. S6). The PXRD patterns of compounds **2** and **3** after exposed to solvents were the same with the as-synthesized compounds, indicating the stability of the compounds in these solvents. For compound **1**, some peaks were shifted in PXRD pattern after exposed to water. The result could be assigned structural changes of compound **1** in water. However, the major part of the PXRD pattern had structure identical with the pristine compound. For the detection studies, the solutions of metal ions (10^{-2} M) were prepared in water and methanol. The solutions of metal ions (0.3 mL, 10^{-2} M) were separately added into the compounds dispersed in water (compounds **1** and **2**) or methanol (compound **3**) and the luminescence spectra of the compounds were taken to determine the effect of metal ions on the emission intensities of the compounds. The emission intensities of the compounds remained largely unaffected in the presence of the other metal ions except for Fe^{3+} ions, which led to the quenching of the luminescence intensities of compounds **1–3** (Fig. 4).

Moreover, the water suspension of the free ligand H_4L free ligand was prepared and its detection ability towards Fe^{3+} ions was studied. The emission intensity of H_4L suspension decreased with the addition of Fe^{3+} ions (0.3 mL, 10^{-2} M) (Fig. S14). The decrease could be due to the coordination of Fe^{3+} to H_4L ions. When compared to quenching efficiencies (43.45% for H_4L), compounds **1–3** displayed higher quenching in the presence of Fe^{3+} ions. The results indicated the promising sensitivity of compounds **1–3** towards Fe^{3+} ions.

To get into sight of the sensitivity of compounds **1–3** towards Fe^{3+} ions, titration studies were conducted with the incremental addition of Fe^{3+} ions (10 µL, 10^{-2} M) to the suspensions of the compounds (1.0 mg, 2.7 mL) (Fig. S15). The results showed that the emission intensities of the compounds decreased step by step with increasing amounts of Fe^{3+} ions. The quenching efficiencies of compounds **1–3** were found to be 88.11%, 63.15% and 89.12% respectively, when Fe^{3+} concentration reached 526 µM. The quantitative detection capabilities of the compounds were also evaluated towards Fe^{3+} ions with the Stern-Volmer (S-V) equation. As seen in Fig. 5, the S-V plots of compounds **2** and **3** were linear at low Fe^{3+} concentrations and deviated from linearity at higher concentrations while the S-V plot of compound **1** was nearly linear at all concentrations. S-V quenching constants of compounds **1–3** for Fe^{3+} ions calculated at low concentrations were 9.58×10^3 M^{-1}, 3.347×10^3 M^{-1} and 6.635×10^3 M^{-1}, respectively. Moreover, the limits of detection were calculated as 2.31 ppm for **1**, 5.17 ppm for **2** and 2.61 ppm for **3**. These results were compatible with some coordination polymers for the detection of Fe^{3+} ions (Table S4).

Besides the sensitive detection of Fe^{3+} ions by the compounds, selective detection of Fe^{3+} ions is crucial for the real environment. At the selectivity studies, the luminescence spectra of the compounds before and after Fe^{3+} ions in the presence of the other competing metal ions were recorded (Fig. 6). As shown in Fig. 6, even in the presence of the other interfering metal ions, Fe^{3+} ions give rise to quenching of the emission intensities of the compounds, demonstrating the selectivity of the compounds towards Fe^{3+} ions in the luminescence detection studies.

For the chemosensor materials, the recyclability possesses an important effect for long-lasting applicability. In the reusability studies, the detection performances of the compounds were evaluated up to five cycles (Fig. S16). The suspension of the compounds before and after exposure to Fe^{3+} ions, the emission spectra of the compounds were recorded and recovered through centrifugation, followed by washing with the solvents. The results showed that the initial emission intensities of compounds **1–3** decreased by 29.6%, 27.0% and 26.4% at the end of five repetition cycles, respectively. The compounds could be reliable candidates for detecting Fe^{3+} ions until three cycles.

Luminescence quenching of the compounds in detecting Fe^{3+} ions was evaluated with diverse detection mechanisms. The PXRD patterns of compounds **2** and **3** were identical with the as-synthesized compounds while the PXRD pattern of compound **1** was not the same as the as-synthesized compound after being exposed to Fe^{3+} ions (Fig. S6). The results showed the stability of the frameworks of compounds **2** and **3** except that the framework of compound **2** could be collapsed at the end of five repetition cycles or partial trans-metalation of iron ion with the Zn(II) ion which had labile coordination bonds could be possible. The framework

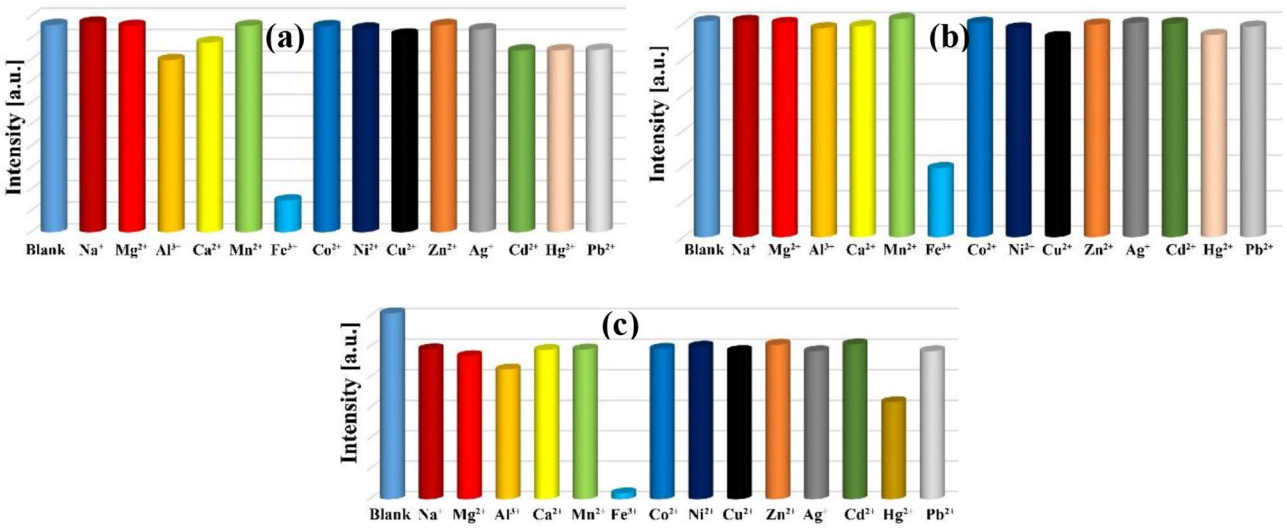

Fig. 4 The luminescence intensity histograms of compounds **1** (**a**), **2** (**b**) and **3** (**c**) in the presence of diverse metal ions (10^{-2} M, 300 µL)

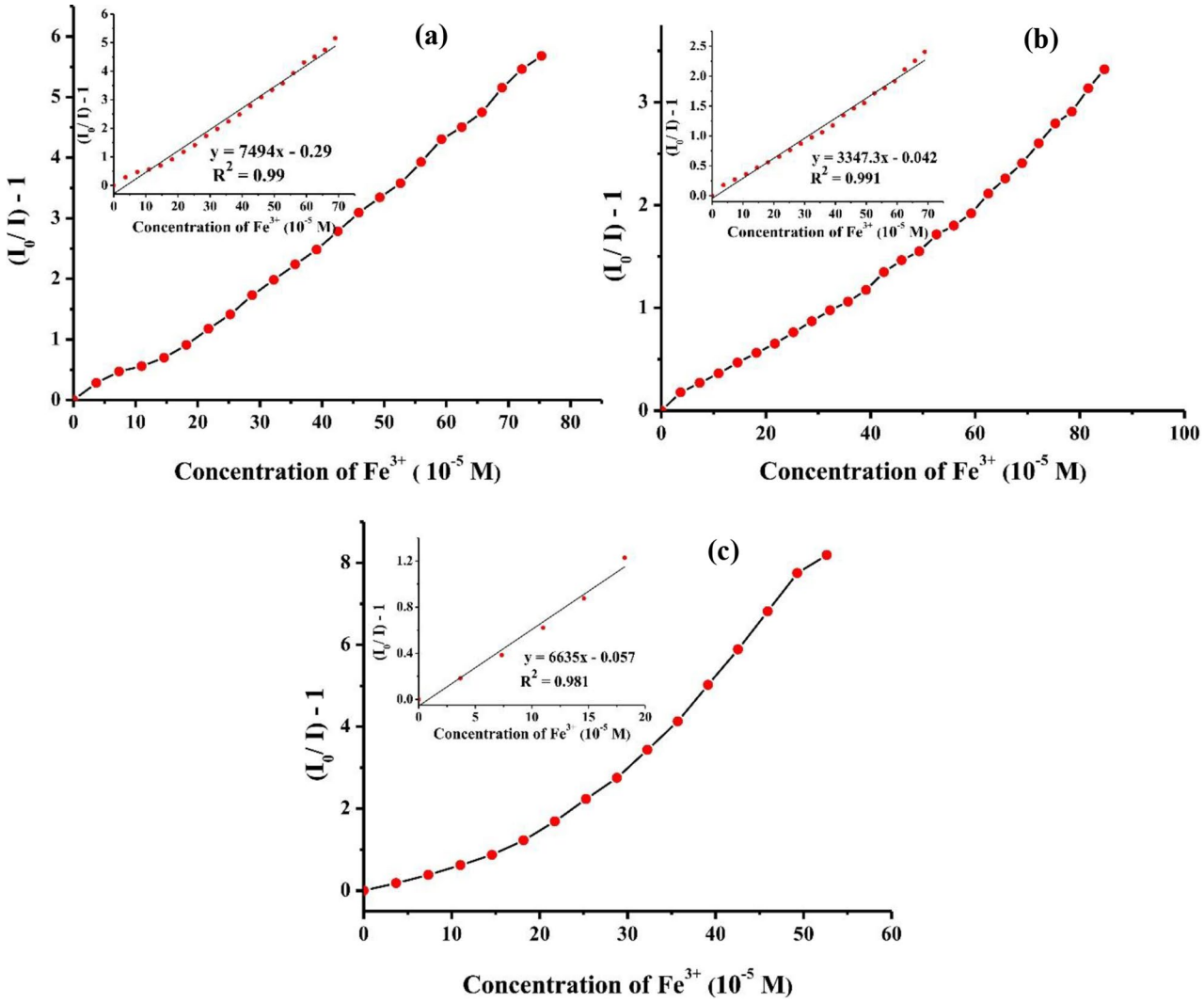

Fig. 5 Stern-Volmer curves of compounds **1** (**a**), **2** (**b**) and **3** (**c**) with incremental addition of Fe^{3+} ions. Emission quenching linearity relationship (inset)

collapsing of compounds **2** and **3** could be eliminated in the detection mechanism. EDX spectra of the compounds after immersing in Fe^{3+} solution were recorded (Fig. S17). EDX spectra of compounds **2** and **3** indicated the existence of a low amount of iron ions, which could be residual Fe^{3+} ions on the surfaces of the compounds. Hence, the ion exchange process for compounds **2** and **3** could be excluded from the detection mechanism of Fe^{3+} ions. However, EDX spectrum of compound **1** showed the presence of higher Fe^{3+} ions when compared to the other compounds. The excitation spectra of the compounds and the absorption spectra of the metal ions were recorded to evaluate the competitive absorption and resonance energy transfer mechanisms. The spectral overlap between the absorption spectrum of a metal ion and the emission spectrum of a sample demonstrates the resonance energy transfer or self-assembly [33]. As seen in Fig. S18a, there is no effective spectral overlap between the absorption spectrum of Fe^{3+} ion and the emission spectra of the compounds, indicating that the resonance energy transfer mechanism can be excluded for the luminescence quenching. However, it is evident that the absorption spectrum of Fe^{3+} ions effectively coincides with the excitation spectra of the compounds, indicating the competitive absorption (Fig. S18b). The excitation energies of compounds **1–3** will be absorbed by Fe^{3+} ions which diminish the energy transfer efficiency from the ligands to Zn(II), leading to luminescence quenching. Moreover, linear and non-linear S-V plot can give an information about static or dynamic quenching mechanism. For compound **1**, the linear S-V plot can imply the presence of the static quenching mechanism while the nonlinear behaviors of S-V plots at high concentrations could be due to the presence of simultaneous static and dynamic quenching for compounds **2** and **3** [34, 35].

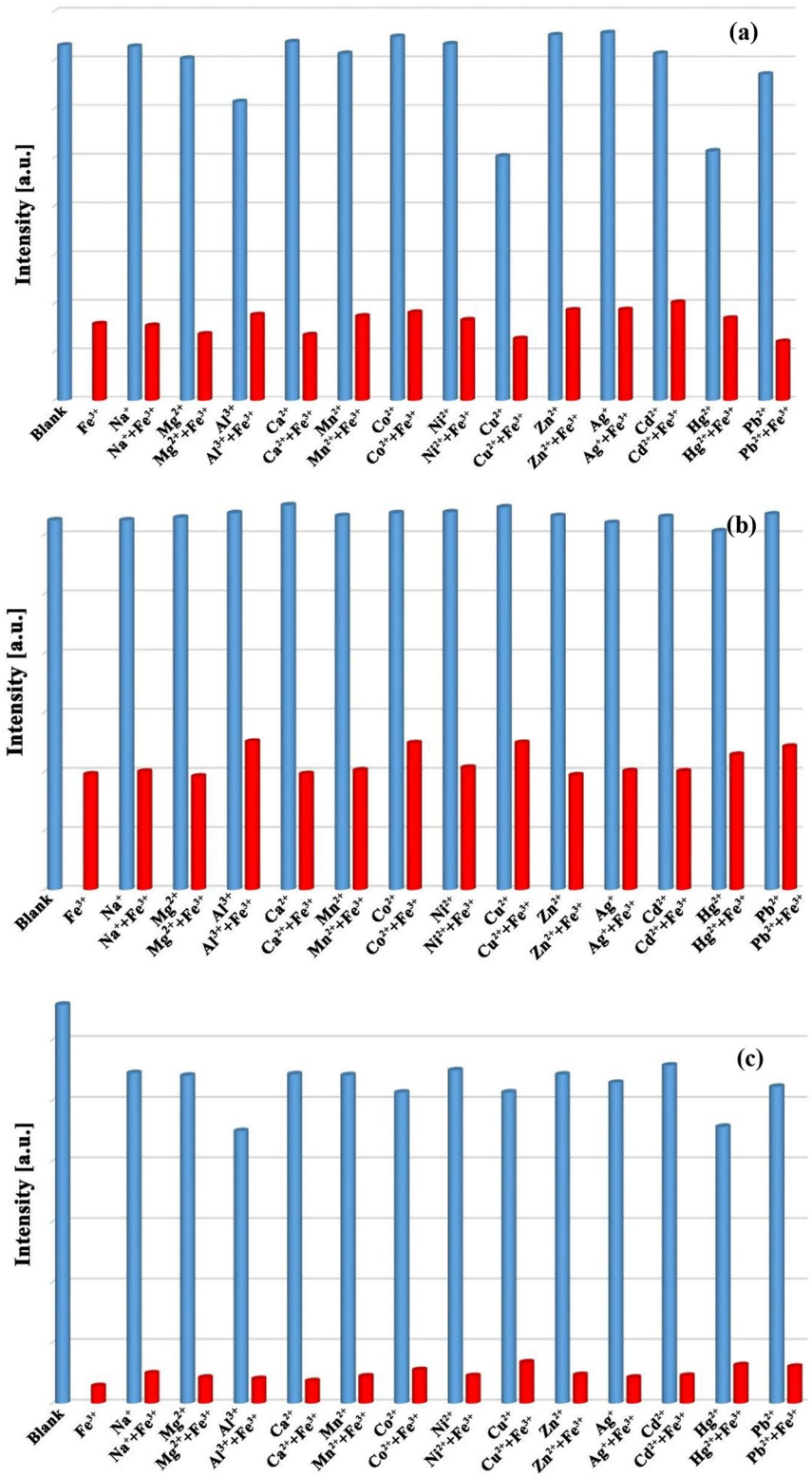

Fig. 6 The change in the luminescence intensities of compounds **1** (**a**), **2** (**b**) and **3** (**c**) in the presence of diverse metal ions before and after addition of Fe^{3+} ions

4 Conclusion

Three new Zn(II)-coordination polymers were synthesized using three isomeric bis(imidazole) linkers and H_4L. In the compounds, 2D and 3D structures were obtained depending on flexible bis(imidazole) ligands while H_4L displayed the same coordination mode in the structures. Compounds **1** and **2** showed 2-fold interpenetrating 3D framework and 2D structure, respectively, although they were synthesized under the same conditions. Compound **3** showed a 4,2-connected 3D structure with 4,4T250 topology. The structural differences could be due to the rotation of imidazole rings around $–CH_2$- groups in bis(imidazole) linkers and dihedral angles between imidazole and phenyl rings in bis(imidazole) linkers. Because the compounds displayed high emission intensities in the solid-state and solution and stability in the solution, the luminescence-based detection of the compounds towards Fe^{3+} was studied. The results showed that the compounds sensitively and selectively detected the Fe^{3+} ions via luminescence quenching with detection limit of 2.31 ppm, 5.17 ppm and 2.61 ppm, respectively. The detection mechanism could be assigned to competitive light absorption between Fe^{3+} ions and the compounds, resulting in luminescence quenching.

Supplementary Information The online version contains supplementary material available at https://doi.org/10.1007/s10904-024-03089-1.

Acknowledgements This work has been supported by Eskisehir Osmangazi University Scientific Research Projects Coordination Unit under grant number FBA-2022-2475.

Author Contributions E.K.: Formal analysis, Investigation, Data curation. Methodology. M.Ş.: Formal analysis, Investigation. A.A.: Formal analysis, Investigation, S.D.: Formal analysis, Investigation, G.S.: Formal analysis, Visualization. F.S.: Investigation, Writing-Review and Editing. H.E.: Formal analysis, Software, Writing-Review and Editing. O.Z.Y.: Investigation, Validation, Writing-Review and Editing. M.A.: Conceptualization, Supervision, Resources, Writing-Review and Editing. All authors reviewed the manuscript.

Funding Open access funding provided by the Scientific and Technological Research Council of Türkiye (TÜBİTAK).

Data Availability No datasets were generated or analysed during the current study.

Declarations

Conflict of interest The authors declare that they have no known competing financial interests or personal relationships that could have influenced the work reported in this paper.

References

1. Z. Lin, J.J. Richardson, J. Zhou, F. Caruso, Nat. Rev. Chem. **7**, 273 (2023)
2. K. Fan, C. Fu, Y. Chen, C. Zhang, G. Zhang, L. Guan, M. Mao, J. Ma, W. Hu, C. Wang, Adv. Sci. **10**, 2205760 (2023)
3. G. Chakraborty, I.-H. Park, R. Medishetty, J.J. Vittal, Chem. Rev. **121**, 3751 (2021)
4. J. Dhainaut, M. Bonneau, R. Ueoka, K. Kanamori, S. Furukawa, ACS Appl. Mater. Interfaces. **12**, 10983 (2020)
5. A. Ahmad, S. Khan, S. Tariq, R. Luque, F. Verpoort, Mater. Today. **55**, 137 (2022)
6. U. Shahzad, H.M. Marwani, M. Saeed, A.M. Asiri, R.H. Althomali, M.M. Rahman, J. Energy Storage. **74**, 109518 (2023)
7. S. Demir, T. Alp Arici, H. Erer, Cryst. Growth \& Des. **23**, 8745 (2023)
8. M. Şevik, S.M. Sezdi, E. Kavak, T.A. Arici, M. Arici, Cryst. Growth Des. **23**, 5163 (2023)
9. E. Çiftçi, T.A. Arıcı, M. Arıcı, H. Erer, O.Z. Yeşilel, J. Solid State Chem. **311**, 123111 (2022)
10. C. Deng, L. Zhao, M.-Y. Gao, S. Darwish, B.-Q. Song, D. Sensharma, M. Lusi, Y.-L. Peng, S. Mukherjee, M.J. Zaworotko, ACS Mater. Lett. **6**, 56 (2023)
11. K. Jomova, M. Makova, S.Y. Alomar, S.H. Alwasel, E. Nepovimova, K. Kuca, C.J. Rhodes, M. Valko, Chem. Biol. Interact. **110173** (2022)
12. S. Ni, Y. Yuan, Y. Kuang, X. Li, Front. Immunol. **13**, 816282 (2022)
13. T. Alp Arici, O.Z. Yesilel, M. Arici, J. Taiwan. Inst. Chem. Eng. **114**, 300 (2020)
14. S.L. Pandrangi, P. Chittineedi, R. Chikati, J.R. Lingareddy, M. Nagoor, S.K. Ponnada, Am. J. Cancer Res. **12**, 974 (2022)
15. T.K. Pal, Mater. Chem. Front. **7**, 405 (2023)
16. L. Tom, M.R.P. Kurup, J. Mater. Chem. C **8**, 2525 (2020)
17. Y.-C. He, H.-L. Yu, K.-Y. Zhao, Y. Wang, C.-S. Geng, S. Wu, H.-K. Yang, F.-H. Zhao, CrystEngComm. **25**, 328 (2023)
18. Y. Zhang, L. Gao, S. Ma, T. Hu, Spectrochim Acta Part. Mol. Biomol. Spectrosc. **267**, 120525 (2022)
19. Q.-L. Cao, R.-T. Wang, J.-Y. Duan, G.-Y. Dong, J. Solid State Chem. **307**, 122816 (2022)
20. B. Wang, Q. Yang, C. Guo, Y. Sun, L.-H. Xie, J.-R. Li, ACS Appl. Mater. Interfaces. **9**, 10286 (2017)
21. Y.S. Kim, J.J. Lee, S.Y. Lee, T.G. Jo, C. Kim, RSC Adv. **6**, 61505 (2016)
22. H.-Q. Yin, X.-B. Yin, Acc. Chem. Res. **53**, 485 (2020)
23. L. Chen, D. Liu, J. Peng, Q. Du, H. He, Coord. Chem. Rev. **404**, 213113 (2020)
24. B. Yan, Inorg. Chem. Front. **8**, 201 (2021)
25. B. Jie, H. Lin, Y. Zhai, J. Ye, D. Zhang, Y. Xie, X. Zhang, Y. Yang, Chem. Eng. J. **454**, 139931 (2023)
26. S.-L. Yao, T.-F. Zheng, X.-M. Tian, S.-J. Liu, C. Cao, Z.-H. Zhu, Y.-Q. Chen, J.-L. Chen, H.-R. Wen, CrystEngComm. **20**, 5822 (2018)

27. H. Yu, Q. Liu, J. Li, Z.-M. Su, X. Li, X. Wang, J. Sun, C. Zhou, X. Hu, J. Mater. Chem. C **9**, 562 (2021)
28. B.B. Rath, J.J. Vittal, Inorg. Chem. **59**, 8818 (2020)
29. E. Kavak, M. Sevik, M. Arici, J. Photochem. Photobiol Chem. **445**, 115032 (2023)
30. H. Erer, O.Z. Yeşilel, M. Arici, Cryst. Growth Des. **15**, 3201 (2015)
31. D. Hu, R. Kluger, Biochemistry. **47**, 12551 (2008)
32. L. Yang, D.R. Powell, R.P. Houser, Dalt Trans. 955 (2007)
33. M. Arici, New. J. Chem. **43**, 3690 (2019)
34. L. Fan, D. Zhao, B. Li, F. Wang, Y. Deng, Y. Peng, X. Wang, X. Zhang, Spectrochim Acta Part. Mol. Biomol. Spectrosc. **264**, 120232 (2022)
35. B. Parmar, K.K. Bisht, Y. Rachuri, E. Suresh, Inorg. Chem. Front. **7**, 1082 (2020)